Applied Nanoscience (2022) 12:725–734
https://doi.org/10.1007/s13204-021-01722-w

ORIGINAL ARTICLE

Adsorption affinity of Zn (II) ions for nanostructured zirconium phosphate/silica or titania composites

W. Janusz[1] · V. Sydorchuk[2] · E. Skwarek[1] · S. Khalameida[2] · J. Skubiszewska-Zięba[1] · R. Leboda[1]

Received: 31 December 2020 / Accepted: 31 January 2021 / Published online: 19 February 2021

Abstract

The paper presents the kinetics of Zn (II) ions adsorption as well as its dependence as a function of pH on nanostructured zirconium phosphate and its composites with silica and titania. The nanostructured zirconium phosphate-containing composites were obtained by mechanical processing in the Pulverisette-7 (Fritsch Gmbh) mill. The obtained composites were characterized by a heterogeneous surface coverage of silica gel or titanium oxides. Zinc ions adsorption studies on these adsorbents showed practically complete removal of Zn (II) from aqueous solutions with an initial concentration of < 0.0001 mol/dm^3 and a pH > 4 within 10 min.

Keywords Adsorption Zn (II) · Nanostructured zirconium phosphate · SiO_2 · TiO_2

Introduction

The development of civilization related to the consumption of modern products causes an increased demand for heavy metals and their compounds. Their production and processing are made in various industries which in the technological processes related to production generate wastes containing heavy metals. These wastes include sewages treated before they are discharged into the environment. To treat wastewaters containing heavy metals, chemical precipitation in the form of insoluble compounds combined with sedimentation or filtration, ion exchange, electrodialysis, flotation, reverse osmosis, ultrafiltration or adsorption are used (Fua and Wang 2011; Renu et al. 2017; de Dias et al. 2019; Altunay et al. 2020; Aboobakri and Jahani 2020; Chen and Wang 2004; Shirsath and Shirivastava 2015; Kaur 2016). Another application of the adsorption methods on new composite materials is the preconcentration of metals species in the chemical analysis (Kaur 2016) or the preparation of new catalysts (Chiang et al. 2019). Adsorption on new composite materials can also be used to remove other troublesome pollutants in sewage and water, such as dyes (Wiśniewska et al. 2018).

. The adsorption of heavy metal ions is a cheap and effective method of removing metal ions from wastewaters and waters contaminated with these metals consisting in using various adsorbents of natural and synthetic origins (Lim et al. 2013; Falayi et al. 2014; Tan et al. 2018; Theron et al. 2008).

Zinc is a micronutrient, the presence of which is essential for the proper functioning of the human body but its overdose may lead to its poisoning. A zinc overdose is especially dangerous for animals (Kabata et al. 1999). Due to overdosing, zinc ions are among those whose concentration is controlled in the environment. Zinc is an element commonly found in the earth's crust but its significant amounts are emitted from metallurgical and processing plants. Moreover, it is used in alloys, anti-corrosion coatings, in the paint, pharmaceutical and cosmetic industries. Soluble zinc salts get into the water and hence it can be absorbed and bioaccumulated by living organisms (Altunay et al. 2020; Eisler 1993).

Studies of the adsorption of zinc ions on the interface metal oxide (SiO_2, Fe_2O_3 and TiO_2)/electrolyte solution as a function of pH showed that in the narrow pH range, cation adsorption increases rapidly creating an adsorption edge (Janusz et al. 2000, 2003; Chibowski et al. 2002). The adsorption edge is characterized by the $pH_{50\%}$ parameter, i.e. the pH value at which 50% of the total amount of cations is

✉ E. Skwarek
ewunias@hektor.umcs.lublin.pl

[1] Faculty of Chemistry, Maria Curie-Skłodowska University, Maria Curie-Skłodowska Sq. 3, 20031 Lublin, Poland

[2] Institute for Sorption and Problems of Endoecology NAS of Ukraine, Naumova Street 13, Kiev 03164, Ukraine

adsorbed. Besides, the $\Delta pH_{10-90\%}$ parameter is related to the pH range in which the cation adsorption increases from 10 to 90% and characterized by the slope of the adsorption edge (Robertson et al. 1997). For the above-mentioned oxides, the $pH_{50\%}$ of the adsorption of zinc ions from the solutions with an initial concentration of 0.000001 mol/dm^3 which characterizes the affinity of ions for the surface, was: 6.2 for SiO_2 (Falayi et al. 2014). 6.5 for α-Fe_2O_3 (Lim et al. 2013) and 5.1 for TiO_2 (Chen and Wang 2004). The tested adsorbents can effectively remove zinc ions from neutral or alkaline solutions.

Due to the higher Bronsted acidity, zirconium phosphate ZrP is promising as an adsorbent of cations (Naushad 2009; Clearfield 1982). However, amorphous ZrP is characterized by a high specific surface area but low accessible due to a sufficiently large content of micropores which impairs its kinetic characteristics and reduces the efficiency of its application in the cation-exchanging processes. The creation of composite materials is one of the ways to overcome this disadvantage. Particularly, the deposition onto the supports with a large specific surface area and developed mesoporosity is one of the most effective methods to improve ZrP properties (Zhang et al. 2008a, b; Perlova et al. 2017). It should be noted that mechanochemical method was previously used for the improvement of adsorption properties both of bulk and supported phosphorus-containing adsorbents (Janusz et al. 2010; Zakutevskyy et al. 2020).

This paper presents the studies of the kinetics and statics of zinc ions adsorption on zirconium phosphate (ZrP) and its composites with SiO_2 or TiO_2, the synthesis and properties of which were described in our previous papers (Khalameida et al. 2017; Sydorchuk et al. 2012).

Experimental

Reagents

Fumed silica (aerosils A-50 and A-380) and titania (Oriana, Ukraine) with the specific surface area 45, 346 and 64 m^2 g^{-1}, respectively, were utilized as supports for the preparation of deposited samples. Aerosils are amorphous and titania consists of anatase and rutile phases.

Synthesis procedures

The procedures of ZrP deposition (20%w/w) were as follows:

Appropriate amounts of reagents, namely ZrP dried xerogel or hydrogel with 88% w/w humidity and fumed titania or aerosils A-50 (A-380), were subjected to mechanochemical treatment (MChT) (milling) at 300 rpm for 0.5 h via Pulverisette-7 (Fritsch Gmbh). The milling was carried out on air (dry milling) or in water (wet milling). Water was not added into the mill when ZrP hydrogel was used. After the wet milling, the dispersions were dried at 20 °C for 72 h. The bulk ZrP, used during milling was prepared through precipitation by H3PO4 from aqueous solutions of ZrOCl2·8H2O as in (Janusz et al. 2000).

Study of physical–chemical characteristics

The starting reagents and products of their mechanochemical transformations were studied by means of X-ray powder diffraction (XRD) using a diffractometer Philips PW 1830 with CuKα- radiation. The FTIR spectra in the range 4000–1400 cm^{-1} were registered using the spectrometer "Spectrum-One" (Perkin-Elmer). The ratio of the sample and KBr powders was 1:20. KBr was dried at 600 °C for 2 h before the measurements.

SEM and EDS analysis

The zirconium phosphate samples and the ZrP/SiO_2 and ZrP/TiO_2 composites were covered with a conductive carbon coater, mounted in the specimen holder and transferred to the Quanta 3D FEG scanning electron microscope, FEI Company. The qualitative and quantitative surface analyses of the main elements of zirconium phosphate samples were conducted from the EDS spectra collected using the FEI Quanta 3D FEG scanning electron microscope equipped with the EDS spectrometer.

Analysis of porous structure

The parameters of porous structure (specific surface area S, sorption pore volume V_s, micropores volume V_{mi}, mesopores volume V_{me}) were determined from the isotherms of low-temperature nitrogen adsorption obtained by means of the analyzer ASAP 2405 N ("Micromeritics Instrument Corp"). The outgassing temperature and duration were 150 °C and 2 h, respectively. Meantime the value of V_s was determined at the relative nitrogen pressure close to 1, the values of V_{mi} and V_{me} were calculated using the t-method and the BJH-method, respectively. The total pore volume V_Σ was determined via impregnation of the samples by liquid water, previously dried at 150 °C. The following relations are valid between these parameters:

$$V_s = V_{mi} + V_{me}$$

$$V_\Sigma = V_s + V_{ma},$$

whereV_{ma}—the volume of macropores which are not filled in the process of adsorption from the vapour phase but filled by impregnation from the liquid phase.

The mesopore diameter dPSD was calculated from the curves of the pore size distribution (PSD) using the desorption branch of isotherms according to the BJH-method.

Zn (II) adsorption measurements

The adsorption densities of Zn (II) ions were measured using the radiotracer technique (Zn-65 radioisotope) was submitted by OPiDI (Świerk, Poland). Based on the radioactivity changes before and after the sorption of Zn (II) ions on the surface of zirconium phosphate samples, adsorption was calculated. The details of the method are described in the literature (Janusz and Skwarek 2018). To compare the adsorption affinity, the ZrP, ZrP/SiO_2 or ZrP/TiO_2 samples were added to 50 ml of Zn (II) ions solution so that the total surface area of the sample to volume ratio of the solution was the same. Radioactivity of the electrolyte solution before and after adsorption was measured using the liquid scintillation counter by Beckman, USA.

Results and discussion

Physicochemical characteristics

The XRD analysis shows that ZrP bulk precipitated in acid medium is X-ray amorphous (Kabata et al. 1999; Janusz et al. 2000; Zhang et al. 2008a, b). Its mechanochemical deposition onto the fumed oxides does not phase the composition of prepared compositions. Thus, the samples based on aerosils retain being X-ray amorphous since both components are the same. On the other hand, the XRD patterns for the TiO_2 samples contain peaks of anatase and rutile as for the support itself. Since the obtained diffraction patterns are not very informative, they are not shown here.

Figure 1a and b show SEM micrographs of samples of zirconium phosphate composites with A380 and A50 aerogels, respectively. SEM micrographs indicate aggregation of large and small particles in composites obtained as a result of mechanochemical treatment of samples. In the case of the ZrP/A380 composite, there is a visible presence of large non-uniform particles in size (~ 400 nm) and shape, and small almost spherical particles, more homogeneous in size (~ 36 nm). The sample of the ZrP/A50 composite, Fig. 1b, obtained as a result of the mechanochemical treatment, also indicates the heterogeneity of the size and shape. However, large particles with a size of ~ 700 nm show a distinct character of small particle agglomerates with a spherical shape and similar size, ~ 65 nm.

The morphology of the particles of zirconium phosphate/titanium oxide composites obtained as a result of mechanochemical treatment is shown in Fig. 2a–c for the samples: 20% $Zr(HPO_4)_2/TiO_2$ MChT of $Zr(HPO_4)_2$ xerogel in air, 20% $Zr(HPO_4)_2/TiO_2$ MChT of $Zr(HPO_4)_2$ xerogel in the water at 300 rpm during 0.5 h and samples 20% $Zr(HPO_4)_2/TiO_2$ MChT of $Zr(HPO_4)_2$ MChT hydrogel in the water at 300 rpm during 0.5 h, respectively. Each of the presented Figures shows a fraction of larger spherical particles with a diameter of ~ 130 nm and a fraction of spherical particles with a smaller diameter ~ 57 nm in the case of the treatment of xerogel samples in air or particles with a diameter of ~ 75 nm of composites mechanically processed in water.

The results of the analysis of the surface composition of ZrP/SiO_2 and ZrP/TiO_2 samples by the EDS method are presented in Table 1. As can be seen, the content of ZrP on the surface of the composites reaches a few percent. This means that only a part of the surface of the SiO_2 or TiO_2

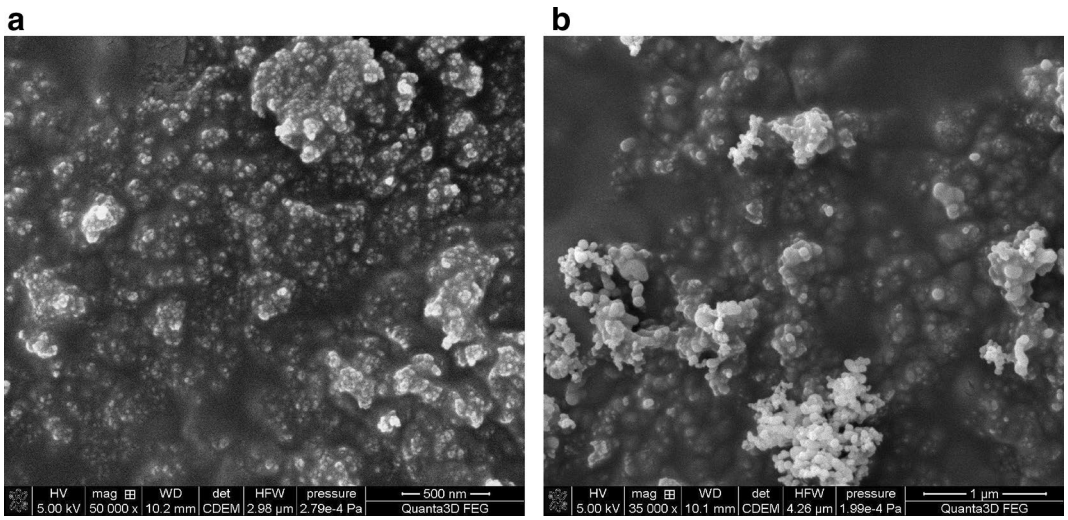

Fig. 1 **a** SEM micrographs of the sample Zr/A380. **b** SEM micrographs of the sample Zr/A50

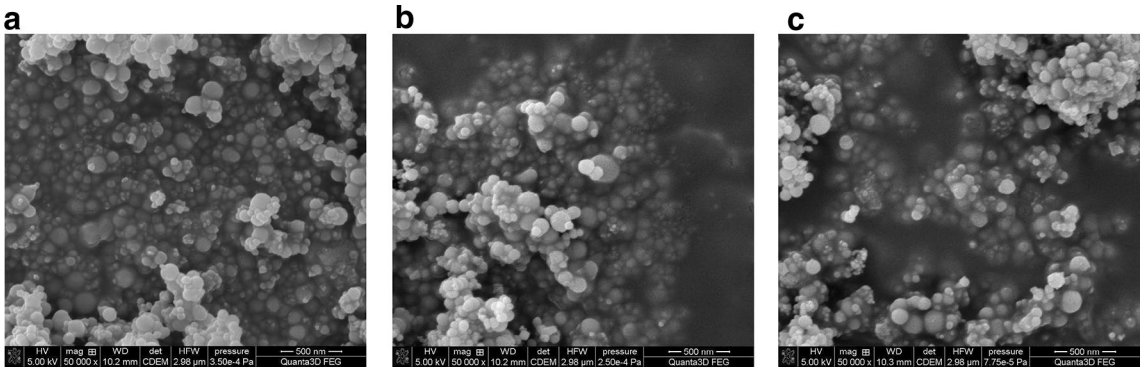

Fig. 2 **a** SEM micrographs of the sample ZrP/TiO_2 xero air. **b** SEM micrographs of the sample ZrP/TiO_2 xero water. **c** SEM micrographs of the sample ZrP/TiO_2 hydrogel water

support is covered with ZrP. Moreover, the analysis of the data presented in Table 1 shows that the ZrP/SiO_2 composite milled in the air (sample 2) is characterized by the lowest content of ZrP on the ZrP/SiO_2 surface. The highest surface ZrP content among ZrP/SiO_2 composites was obtained by the method of mechanical treatment of the mixture containing ZrP in the form of a wet gel (sample 6).

In the case of ZrP/fumed TiO_2 composites, mechanical treatment in the air also leads to the smallest surface content of ZrP, although the difference between the samples, mechanically treated in water and in the air (samples 4 and 3, respectively), is smaller. This difference can be explained as follows. Taking into account a large excess of silica in relation to ZrP, as well as the difference in the hardness of the components (Mohs hardness of amorphous silica and ZrP is 5 and 6.5, respectively) (Wood and Hodgkiess 1972; Davraz and Gunduz 2005), "smearing" of amorphous silica on the ZrP particles is possible during dry milling. To a lesser extent, this applies to the composition based on crystalline TiO_2. If the phase, that is deposited (ZrP), is in the form of a wet gel (samples 6 and 7), the Zr/Si(Ti) ratio is 1.5–2 times higher than during deposition of a dried ZrP xerogel (samples 2–4). Similar results were obtained during the mechanochemical deposition of tin dioxide on silica gel (Khalameida et al. 2020).

The FTIR spectra of the studied samples for the range 4000–1400 cm^{-1}, presented in Figs. 3 and 4, confirm the results of EDS analysis. As can be seen, these spectra contain broad absorption bands (a.b.) at 3800–2700 cm^{-1} which consist of several components and are attributed to the stretching vibrations of the surface OH-groups. Particularly, the spectra recorded for samples based on aerosils contain sharp a.b. at 3745 cm^{-1} and broad a.b. with the maximum about 3300 cm^{-1}. The former is assigned to the isolated silanol groups (Innocenzi 2003; Skubiszewska-Zieba et al. 2016; Christy 2011) and the latter—to the P–OH groups Zhang et al. 2008a, b; Pica 2017; Rao et al. 2017; Jastrzębski et al. 2011). Similarly, the spectra for samples based on TiO_2 contain a.b. at 3550 cm^{-1} and 3300 cm^{-1}. The first of these bands is attributed to the stretching vibrations of Ti–OH groups (Deiana et al. 2010; Cerrato et al. 1993). Therefore, the spectroscopic data show that the deposited ZrP phase does not cover completely the surface of the support and the surface of the compositions has a mosaic structure.

Bulk ZrP has a micro-mesoporous structure (Sydorchuk et al. 2012). Its mechanochemical deposition onto fumed oxides in water facilitates meso-macroporous compositions formation. As a result, the isotherms characteristic for mesoporous materials were recorded for these supported samples (Rouquerol et al. 1994). Besides, PSD curves have several maxima in the range of mesoporosity [inset to Fig. 1 in Sydorchuk et al. (2012)]. The parameters of their porous structure are listed in Table 2. One can see that sample 2 prepared by dry milling possesses a maximal specific surface area. This milled sample is a highly dispersed and nonporous powder, as found by dry milling of pure aerosil in work (Sydorchuk et al. 2010). The other studied samples have developed mesoporous or meso-macroporous structure i.e. they are characterized by the multimodal porosity which accelerates diffusion in porous space. The excess of the V_Σ value over the V_s one confirms the presence of macropores. As a result, porous structure of deposited compositions and cation-exchanged sites should be more accessible for hydrated Zn species.

Kinetics of Zn (II) adsorption on ZrP

The kinetics of zinc ions adsorption on the ZrP/SiO_2 composite samples from a solution with an initial concentration of Zn (II) ions of 0.000001 mol/dm^3 and an initial concentration of 0.0001 mol/dm^3 are presented, in Figs. 5 and 6, respectively. Obviously, the faster kinetics for the supported samples compared with bulk ZrP is due to their multimodal porosity: the absence of micropores

Tabel 1 EDS analysis results

Sample. No	Synthesis	Element %At								P/Zr	*Zr/Si(Ti)*
		C *K*	N *K*	O *K*	Na *K*	Mg *K*	Si *K*	P *K*	Zr *K*		
1	$Zr(HPO_4)_2$ bulk. precipitation from $ZrOCl_2$ and H_3PO_4			67.4				18.2	14.1	1.30	
ZrP/SiO_2 composites											
2	20% $Zr(HPO_4)_2$/A-380. MChT of $Zr(HPO_4)_2$ xerogel on air. 300 rpm 0.5 h	10.8	2.6	50.9	0.0		34.0	0.8	0.9	0.83	0.03
6	20% $Zr(HPO_4)_2$/A-50. MChT of $Zr(HPO_4)_2$ hydrogel in water. 300 rpm 0.5 h		2.9	54.3	0.1	0.1	37.9	2.4	2.4	1.04	0.06
ZrP/TiO_2 composites											
3	20% $Zr(HPO_4)_2/TiO_2$ MChT of $Zr(HPO_4)_2$ xerogel in air. 300 rpm 0.5 h	0.0	53.6	0.4	0.4	11.4	2.3	30.0	2.0	1.14	0.07
4	20% $Zr(HPO_4)_2/TiO_2$ MChT of $Zr(HPO_4)_2$ xerogel in water. 300 rpm 0.5 h	0.0	54.8	0.2	0.3	11.2	2.8	28.4	2.3	1.18	0.08
7	20% $Zr(HPO_4)_2/TiO_2$ MChT of $Zr(HPO_4)_2$ hydrogel in water. 300 rpm 0.5 h	0.0	56.7	0.4	0.4	10.3	3.4	25.6	3.2	1.08	0.12

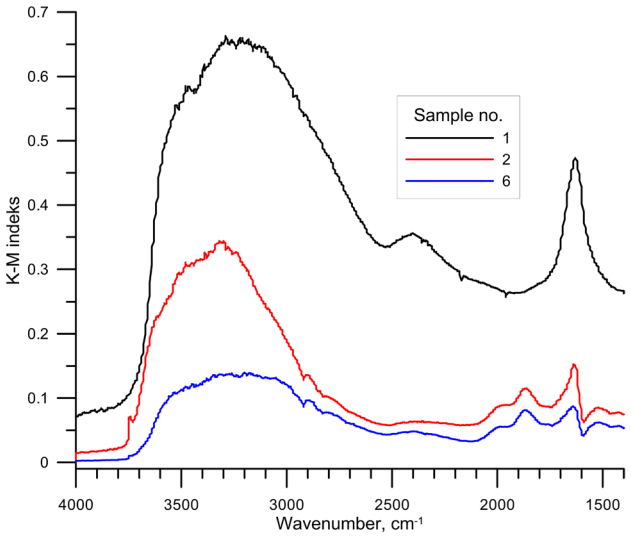

Fig. 3 FTIR spectra of ZrP and ZrP/SiO_2 composites

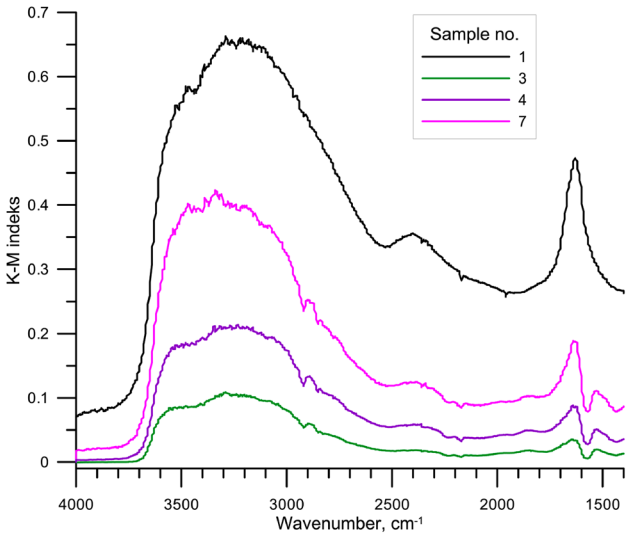

Fig. 4 FTIR spectra of ZrP and ZrP/TiO_2 composites

but the presence of macropores and mesopores of different sizes (Table 2). The latter facilitates fast diffusion of hydrated cations in the pores and accessibility of surface cation-exchanged sites. The pseudo-first-order, pseudo-second-order, intra-particle diffusion and Elovic models were fitted to the time dependence of adsorption, as in works (Tan et al. 2018; Zhang et al. 2008a, b; Shafaati et al. 2020; He et al. 2020; Bulin et al. 2020). The best fit of the experimental results was obtained using the pseudo-second-order model as for sorption of Cd(II) on modified attapulgite (He et al. 2020) or Cr (VI) using reduced graphene oxide/montmorillonite composite (Peng et al. 2020). The comparison of the experimental data (points)

Table 2 Influence of synthesis conditions on the porous structure resulted compositions [Error! Bookmark not defined.]

Sample no	Synthesis	S m^2/g	V_Σ cm^3/g	V_{mi} cm^3/g	V_{me} cm^3/g	V_{ma} cm^3/g	d_{me} nm
1	$Zr(HPO_4)_2$ bulk, precipitation from $ZrOCl_2$ and H_3PO_4	195	0.15	0.07	0.08	–	3.6
ZrP/SiO_2 composites							
2	20 $Zr(HPO_4)_2$/A-380. MChT of $Zr(HPO_4)_2$ xerogel in air, 300 rpm 0.5 h	278	–	–	–	–	–
6	20% $Zr(HPO_4)_2$/A-50. MChT of $Zr(HPO_4)_2$ hydrogel, 300 rpm 0.5 h	107	1.21	–	0.19	1.02	3.3
ZrP/TiO_2 composites							
3	20% $Zr(HPO_4)_2$fumed TiO_2. MChT of $Zr(HPO_4)_2$ xerogel in air, 300 rpm 0.5 h	148	0.44	0.01	0.43	–	3.8; 40
4	20% $Zr(HPO_4)_2$/fumed TiO_2. MChT of Zr(HPO4)2 xerogel in H_2O, 300 rpm 0.5 h	51	0.56	–	0.10	0.46	3.8; 23
7	20% $Zr(HPO_4)_2$/fumed TiO_2. MChT of $Zr(HPO_4)_2$ hydrogel, 300 rpm 0.5 h	84	0.63	–	0.17	0.46	5.5; 50

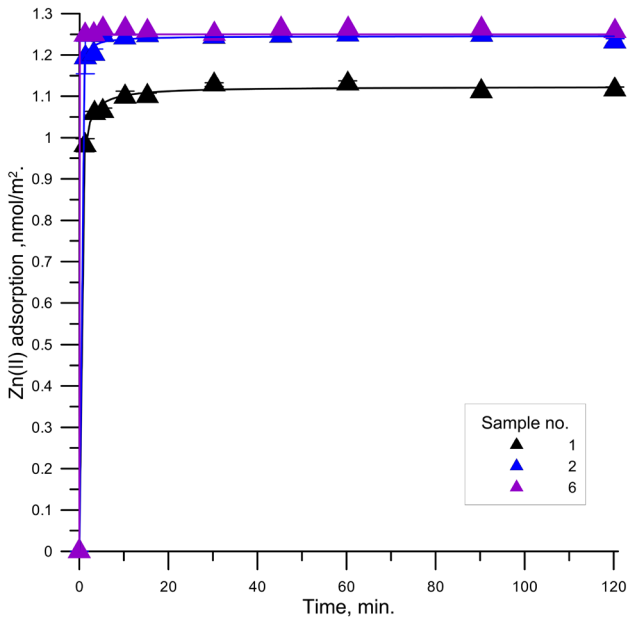

Fig. 5 Kinetics Zn (II) ions adsorption of on the zirconium phosphate/silica (sample no 2 and 6) and zirconium phosphate/titania (sample no4) composites samples from the solution of the initial concentration 0.000001 mol/dm^3 Zn (II) ions. The points indicate the experimental data, the lines-the pseudo-second-order model using the constants collected in Table 3

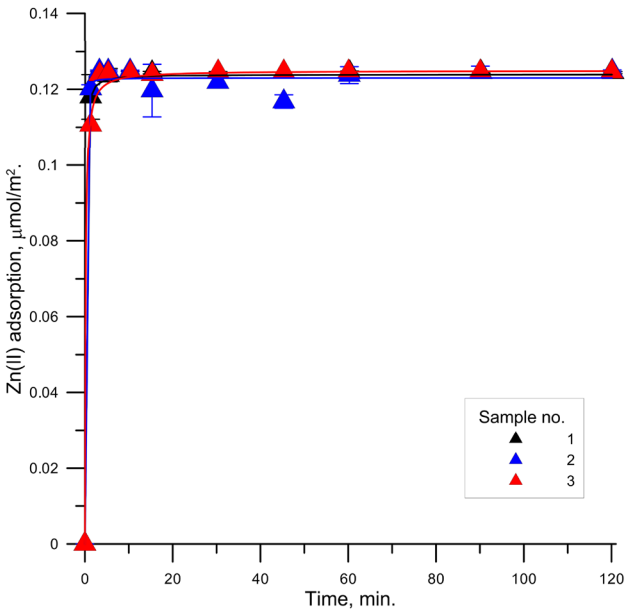

Fig. 6 Kinetics Zn (II) ions adsorption of Zn (II) ions on the zirconium phosphate/silica or titania composites samples from the solution of the initial concentration 0.0001 mol/dm^3 Zn (II) ions. The points indicate the experimental data, the lines-the pseudo-second-order model using the constants collected in Table 4

to the model calculations with the second-order model (lines) is shown in Figs. 5 and 6 (points) and the constants of the fit with the pseudo-second-order model are presented in Tables 3 and 4 for the initial concentrations of 0.000001 and 0.0001 mol/dm^3. As can be seen from the data of Tables 3 and 4, the equilibrium adsorption for all samples is the same except the sample No. 1 (ZrP), namely for the Zn (II) ions adsorption from solution with the initial concentration of 0.000001 mol/dm^3. However, in this case, the adsorption pH, due to the acidic nature of the zirconium phosphate surface groups, was much lower than for the other samples (pH 3 against pH ~ 6, respectively). Since the adsorption of Zn (II) ions takes place through the

Table 3 Constants of the pseudo-second-order model of the kinetics of Zn (II) ions adsorption from the solution of the initial concentration 0.000001 mol/dm^3 on ZrP/silica and ZrP/titania composites

Sample no	k_2	q_{eq}	$\sum\left(\frac{a_e-a_c}{a_e}\right)^2$
1	4.50	1.12	0.0011
2	12.54	1.25	0.0009
3	1634.97	1.25	2.14E-07
6	65.50	1.26	0.0002

exchange of hydrogen ions of surface groups, a lower pH value reduces the adsorption of Zn (II) ions. The presented results of the kinetics of Zn (II) adsorption show that the

Table 4 Constants of the pseudo-second-order model of kinetic Zn(II) ions adsorption from the solution of the initial concentration 0.0001 mol/dm^3 at ZrP/silica and ZrP/titania composites

Sample no	k_2	a_{eq}	$\sum\left(\frac{a_e-a_c}{a_e}\right)^2$
1	128.3	0.125	5.05E-06
2	589.9	0.123	7.35E-05
3	55.1	0.126	2.31E-05

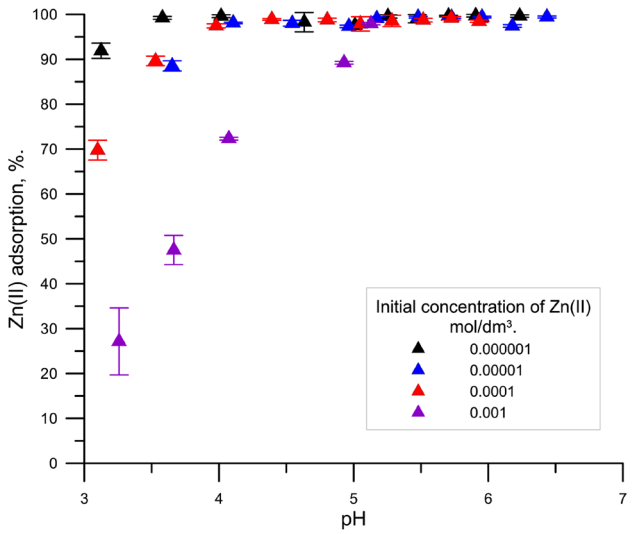

Fig. 7 Adsorption (%) of Zn (II) ions on zirconium phosphate as a function of pH for different initial concentrations of Zn (II) ions

adsorption of zinc ions on both bulk zirconium phosphate and its composites with SiO_2 reaches equilibrium within a few minutes.

The dependence of Zn (II) ions adsorption at the ZrP interface as a function of pH for different concentrations of Zn (II) ions is shown in Fig. 7 while for the ZrP/SiO_2 and ZrP/TiO_2 composites it is presented for the initial concentration of 0.000001 mol/dm^3 Zn (II) ions in Fig. 8, and for the initial concentration of 0.0001 mol/dm^3 in Fig. 9. The course of adsorption of Zn (II) ions at the above-mentioned phase boundaries as a function of pH resembles the adsorption of cations at the interface metal oxide—electrolyte solution interface, which is characterized by the edge adsorption, i.e. a narrow pH range in which the adsorption increases from almost 0–100%. The characteristic parameters of the edge are $pH_{50\%}$ adsorption and $\Delta pH_{10-90\%}$. The first parameter indicates the adsorption affinity of ions for the surface of a solid, the latter determines the slope of the adsorption edge.

The adsorption of cations on zirconium phosphate, similarly to the metal oxide, can be described as a process of

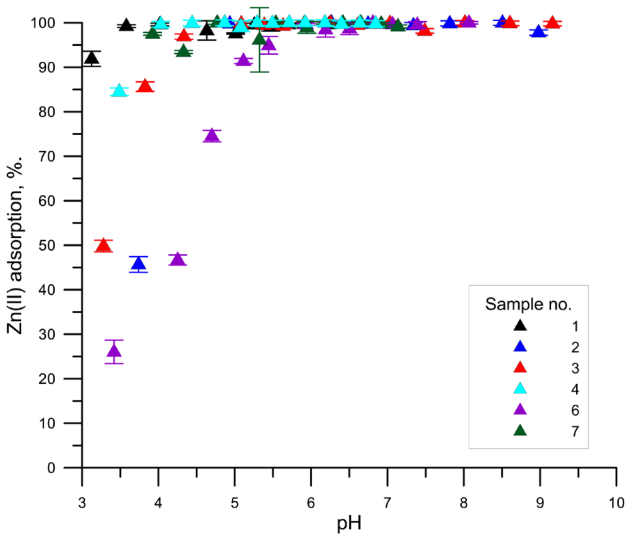

Fig. 8 Adsorption (%) of Zn (II) ions on the zirconium phosphate/silica or titania composites samples from the solution of the initial concentration 0.000001 mol/dm^3 of Zn (II) ions as a function of pH

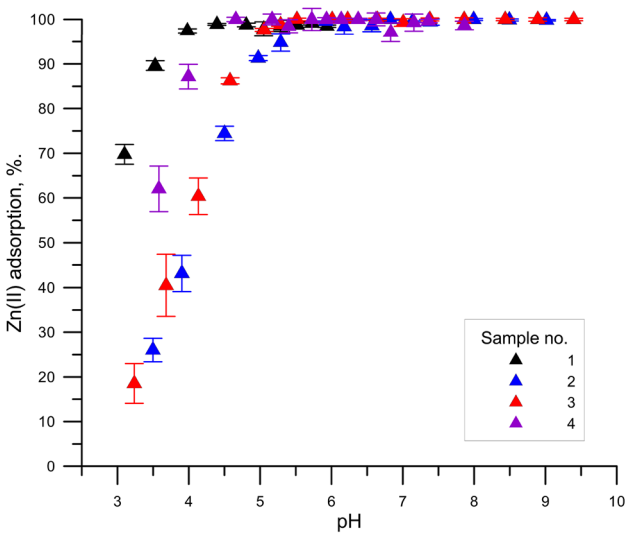

Fig. 9 Adsorption of Zn (II) ions on the zirconium phosphate/silica or the zirconium phosphate/titania composites samples from the solution of the initial concentration 0.0001 mol/dm^3 of Zn (II) ions as a function of pH

non-stoichiometric cation exchange with a hydrogen atom from a surface hydroxyl group on a metal oxide (Bulin et al. 2020).

$$n \equiv SOH + Me^{z+} \Leftrightarrow (\equiv SO^-)_n M^{(z-n)+} + nH^+ \quad (1)$$

Where≡SOH denotes the surface group ZrP (≡ZrOH or = POH).M—denotes the metal cation (Zn^{2+}).*n*—the number of surface groups reacting with the cation = the number

Table 5 Equilibrium constants of Zn (II) adsorption and the amount of released H^+ ions based on the non-stoichiometric exchange model

Sample no	Synthesis	Zn[II] conc. [mol/dm^3]	$p\beta_n^s$	n	$pH_{50\%}$	$\Delta pH_{10-90\%}$
1	$Zr(HPO_4)_2$ bulk. precipitation from $ZrOCl_2$ and H_3PO_4	0.001	0.05	0.8	3.2	2.3
		0.0001	1.18	1.2	2.8	1.5
		0.00001	0.52	1.1	2.7	1.8
		0.000001	3.36	0.9	1.2	2.2
ZrP/SiO_2 composites						
2	20 $Zr(HPO_4)_2$/A-380. MChT of $Zr(HPO_4)_2$ xerogel in air. 300 rpm 0.5 h	0.0001	0.02	1.0	4.0	1.9
		0.000001	0.4	0.9	3.4	2.2
6	20% $Zr(HPO_4)_2$/A-50. MChT of $Zr(HPO_4)_2$ hydrogel. 300 rpm 0.5 h	0.0001	1.1	1.8	3.4	1.16
		0.000001	0.006	0.7	4.1	2.8
ZrP/TiO_2 composites						
3	20% $Zr(HPO_4)_2$fumed TiO_2. MChT of $Zr(HPO_4)_2$ xerogel in air. 300 rpm 0.5 h	0.0001	0.03	1.0	3.9	1.8
		0.000001	0.6	1.4	3.3	1.3
4	20% $Zr(HPO_4)_2$/fumed TiO2. MChT of Zr(HPO4)2 xerogel in H_2O. 300 rpm 0.5 h	0.000001	129.2	2.48	3.1	0.8
7	20% $Zr(HPO_4)_2$/fumed TiO_2. MChT of $Zr(HPO_4)_2$ hydrogel. 300 rpm 0.5 h	0.0001	0.6	1.6	3.2	1.2
		0.000001	0.27	1.07	3.0	1.8

of released H + cations.z—the electric charge of the cation (2 +).

Assuming that the energy of the chemical interactions of the ion with the surface group is much greater than that of the electrostatic interactions, the thermodynamic constant of the cation adsorption reaction on the zirconium phosphate surface, omitting the electrostatic interaction component, can be expressed by the following formula:

$$\beta_n^s = \frac{\left[(\equiv SO^-)_n M^{(z-n)+}\right]\left[H^+\right]^n}{[\equiv SOH]^n\left[M^{z+}\right]} \quad (2)$$

where

β_n^s—the thermodynamic constant of the reaction.

When the equation is logged and transformed, a linear form is obtained that allows to calculate the equilibrium constant of the reaction β_n^s and the n factor related to the amount of released ions H^+:

$$lg\left(\frac{\left[(\equiv SO^-)_n M^{(z-n)+}\right]}{\left[M^{z+}\right]}\right) = \lg(\beta_n^s) + n\lg\left(\frac{[\equiv SOH]}{\left[H^+\right]}\right) \quad (3)$$

The values of the constants and the amount of released H^+ ions obtained by this method change with the concentration of the adsorbed ion and that of the carrier electrolyte. However, a good match of the adsorption as a function of pH is achieved for a given concentration of the ion and the background electrolyte.

The relations presented in Figs. 7–9 show only a part of the adsorption edge. In the case of zirconium phosphate, the adsorption edge is shifted towards the acidic pH scale, the $pH_{50\%}$ calculated using the non-stoichiometric exchange model is 1.2, while the number of H^+ ions exchanged is 0.9. The $pH_{50\%}$ value indicates a very high affinity of Zn (II) ions for the ZrP surface at the initial concentration 0.000001 mol/dm^3 Zn (II): in the case of TiO_2 (anatase) $pH_{50\%} \sim 5.5$ (Janusz et al. 2000, 2003) and for SiO_2 $pH_{50\%} = 6.2$ (Janusz et al. 2003).

The computations of the equilibrium constants of Zn (II) adsorption and the amount of released H^+ ions based on the non-stoichiometric exchange model are presented in Table 5, taking into account the following concentrations of the surface hydroxyl groups: at ZrP surface 4.2 OH groups/nm^2 (Tang et al. 2016), at silica 4.9 OH groups/nm^2 (Zhuravlev 1987) and TiO_2 4.8 OH groups/nm^2 (Wu et al. 2017). In most cases of Zn (II) adsorption on zirconium phosphate and composite materials, the amount released by one Zn (II) ion is approximately equal to 1 H^+ ion. This is an approximate value because the slope of the line representing the relationship lg $\{[(\equiv SO\text{-})_n Zn^{2-n}]/[Zn^{2+}]\}$ vs. lg$\{[H^+]/[\equiv SOH]\}$ apart from the value of n also contains a component of electrostatic interactions. Nevertheless, reaction 1 represents a certain result of the adsorption reaction on one or two functional groups and allows to determine the participation of these reactions in the adsorption of Zn (II) ions and surface groups. In the case of ZrP/SiO_2 composites, $pH_{50\%} = 3.4$ and for ZrP/TiO_2 composites, $pH_{50\%} = 3.1$. This may be due to the contribution of weaker acidic Si–OH and Ti–OH groups (see FTIR data in Figs. 1 and 2). An increase in the initial concentration of Zn (II) ions causes a shift of the adsorption edge towards higher pH values and its flattening (Table 5).

Conclusions

The nanostructured compositions containing 20% zirconium phosphate and 80% silicon dioxide or titanium dioxide prepared through milling the mixture of precipitated zirconium phosphate with fumed oxides at 300 rpm for 0.5 h contain only a few % of zirconium phosphate on the surface and have developed meso- and meso-macroporous structure if milling is carried out in the presence of water. Strong P-OH as well as weak Si–OH and Ti–OH groups are present on their surface. The adsorption of Zn (II) ions on nanostructured zirconium phosphate and its composites with oxides reaches equilibrium within 10 min and is well described by the pseudo-second-order kinetic equation.

Location of the Zn (II) adsorption edge on zirconium phosphate from the solutions with an initial concentration of 0.000001 mol/dm^3, $pH_{50\%}$ falls at pH = 1.3, while for a concentration of 0.001 mol/dm^3 $pH_{50\%}$ = 3.2. These values indicate that bulk zirconium phosphate can remove Zn (II) ions from the aqueous solutions in the acidic environment effectively. Research on the adsorption of Zn (II) ions on the ZrP/SiO_2 and ZrP/TiO_2 composites indicates that these composites can remove Zn (II) ions from aqueous solutions with pH > 5 effectively.

Compliance with ethical standards

Conflict of interest On behalf of all authors, I state that there is no conflict of interests.

References

Aboobakri E, Jahani M (2020) Graphene oxide/Fe3O4/polyaniline nanocomposite as an efficient adsorbent for the extraction and preconcentration of ultra-trace levels of cadmium in rice and tea samples. Res Chem Intermed 46(4):2347–2374

Altunay N, Tuzen M, Hazer B, Elik A (2020) Usage of the newly synthesized poly(3-hydroxy butyrate)-b-poly(vinyl benzyl xanthate) block copolymer for vortex-assisted solid-phase microextraction of cobalt (II) and nickel (II) in canned foodstuffs. Food Chem 321:126690

Bulin C, Li B, Zhang Y, Zhang B (2020) Removal performance and mechanism of Fe_3O_4/graphene oxide as an efficient and recyclable adsorbent toward aqueous Hg(II). Res Chem Intermed 46(3):1–12

Cerrato G, Marchese L, Morterra C (1993) Structural and morphological modifications of sintering microcrystalline TiO2: an XRD, HRTEM and FTIR study. Appl Surf Sci 70:200–205

Chen JP, Wang L (2004) Characterization of metal adsorption kinetic properties in batch and fixed-bed reactors. Chemosphere 54:397–404

Chiang Hsieh LH, Ou HH, Huang ChW (2019) Adsorption of Cu(II) in aqueous solution using microwave-assisted titanate nanotubes. Appl Nanosci 9:505–514

Chibowski S, Janusz W (2002) Specific adsorption of Zn(II) and Cd(II) ions at the α-Fe_2O_3/electrolyte interface-structure of the electrical double layer. Appl Surf Sci 196:343–355

Christy A (2011) Effect of hydrothermal treatment on adsorption properties of silica gel. Ind Eng Chem Res 50:5543–5549

Clearfield A (1982) Inorganic ion exchanger materials. CRC Press, Boca Raton

Davraz M, Gunduz L (2005) Engineering properties of amorphous silica as a new natural pozzolan for use in concrete. Cement Concrete Res 35:1251–1261

de Dias FS, Guarino MEPA, Costa Pereira AL, Pedra PP, de Bezerra MA, Marchetti SG (2019) Multivariate optimization of ultrasound-assisted liquid–liquid microextraction based on two solvents for cadmium preconcentration prior to determination by flame atomic absorption spectrometry. Microchem J 146:1095–1110

Deiana C, Fois E, Coluccia S, Martra G (2010) Surface structure of TiO2 P25 nanoparticles: infrared study of hydroxy groups on coordinative defect sites. J Phys Chem C 114:21531–21538

Eisler R, (1993) Zinc Hazards to Fish, Wildlife, and Invertebrates: A Synoptic Review. Biological Report 10 Contaminant Hazard Reviews, Report 26, U.S. Department of the Interior Fish and Wildlife Service, Patuxent Wildlife Research Center, Laurel, Maryland 20708

Falayi T, Ntuli F (2014) Removal of heavy metals and neutralisation of acid mine drainage with un-activated attapulgite. J Ind Eng Chem 20:1285–1300

Fua F, Wang Q (2011) Removal of heavy metal ions from wastewaters: a review. J Environ Manag 92:407–418

He Y, Sun X, Zhang P, Wang F, Zhao Z, He C (2020) Cd(II) adsorption from aqueous solutions using modified attapulgite. Res Chem Intermed 46(2):1–12

Innocenzi P (2003) Infrared spectroscopy of sol-gel derived silica-based films: a spectra-microstructure overview. J Non-Cryst Solids 316:309–319

Janusz W, Skwarek E (2018) Effect of Co(II) ions adsorption in the hydroxyapatite/aqueous $NaClO_4$ solution system on particles electrokinetics. Physicochem Probl Min 54:31–39

Janusz W, Jabłoński J, Sprycha R (2000) The Electrical interfacial layer at the TiO_2 (anatase)/electrolyte interface – adsorption of Zn(II) and Cd(II) ions. J Dispers Sci Technol 21:739–759

Janusz W, Patkowski J, Chibowski S (2003) Competitive adsorption of Ca^{2+} and Zn (II) ions at monodispersed SiO_2/electrolyte solution interface. J Colloid Interface Sci 266:259–268

Janusz W, Khalameida S, Sydorchuk V, Skwarek E, Zazhigalov V, Skubiszewska-Zięba J, Leboda R (2010) Some properties of milled vanadium phosphates. Adsorption 16(4–5):333–341

Jastrzębski W, Sitarz M, Rokita M, Bułat K (2011) Infrared spectroscopy of different phosphates structures. Spectrochimica Acta Part A Mol Biomol Spect 79(4):722–727

Kabata-Pendias A, Pendias H, 1999, Biogeochemia pierwiastków śladowych, PWN, 344.

Kaur A (2016) Applications of organo-silica nanocomposites for SPNE of Hg(II). Appl Nanosci 6:183–190

Khalameida S, Sydorchuk V, Skubiszewska-Zięba J, Charmas B, Skwarek E, Janusz W (2017) Hydrothermal, microwave and mechanochemical modification of amorphous zirconium phosphate structure. J Therm Anal Calorim 128:795–806

Khalameida S, Sydorchuk V, Levytska S, Shcherban N (2020) Physicochemical and photocatalytic properties of tin dioxide supported onto silica gel. J Therm Anal Calorim 140:2131–2142

Lim AP, Aris AZ (2013) A review on economically adsorbents on heavy metals removal in water and wastewater. Rev Environ Sci Biotechnol 13:163–181

Naushad M (2009) Inorganic and composite ion exchange materials and their applications. Ion Exch Lett 2:1–14

Peng C, He Z, Feng J, Chen D, Ding H, Wang J, Du G (2020) Preparation of reduced graphene oxide/montmorillonite composite hydrogel. Res Chem Intermed 46(12):1–15

Perlova N, Dzyazko Y, Perlova O, Palchik A, Sazonova V (2017) Formation of zirconium hydrophosphate nanoparticles and their effect on sorption of uranyl cations. Nanosc Res Let 12(1):209

Pica M (2017) Zirconium phosphate catalysts in the XXI century: state of the art from 2010 to date. Catalysts 7(6):190

Rao KTV, Souzanchi S, Yuan Z, Ray MB, Xu C (2017) Simple and green route for preparation of tin phosphate catalysts by solid-state grinding for dehydration of glucose to 5-hydroxymethylfurfural (HMF). RSC Adv 7(76):48501–48511

Renu B, Agarwal M, Singh K (2017) Methodologies for removal of heavy metal ions from wastewater: an overview. Interdis Environ Rev 18(2):124–142

Robertson AP, Leckie JO (1997) Cation binding predictions of surface complexation models: effects of pH, Ionic strength, cation loading, surface complex, and model fit. J Colloid Interface Sci 188:444–456

Rouquerol J, Avnir D, Fairbridge CW, Everett DH, Haynes JM, Pernicone N, Ramsay JDF, Sing KSW, Unger KK (1994) Recommendations for the characterization of porous solids. Pure Appl Chem 66(8):1739–1758

Shafaati M, Miralinaghi M, Shirazi RHSM, Moniri E (2020) The use of chitosan/Fe_3O_4 grafted graphene oxide for effective adsorption of rifampicin from water samples. Res Chem Intermed 46(4):2247–2274

Shirsath DS, Shirivastava VS (2015) Adsorptive removal of heavy metals by magnetic nanoadsorbent: an equilibrium and thermodynamic study. Appl Nanosci 5:927–935

Skubiszewska-Zieba J, Khalameida S, Sydorchuk V (2016) Comparison of surface properties of silica xero- and hydrogelshydrothermally modified using mechanochemical, microwave and classical methods. Colloids Surf A Physicochem Eng Aspects 504:139–153

Sydorchuk V, Khalameida S, Zazhigalov V, Skubiszewska-Zięba J, Leboda R, Wieczorek-Ciurowa K (2010) Influence of mechanochemical activation in various media on structure of porous and non-porous silicas. Appl Surf Sci 257:446–450

Sydorchuk V, Janusz W, Khalameida S, Skwarek E, Skubiszewska-Zieba J, Leboda R, Zazhigalov V (2012) Synthesis, structure and some properties of zirconium phosphate/ oxide support compositions. Therm Anal Calorim 108:1009–1016

Tan B, Zhao H, Zhang Y, Quan X, He Z, Zheng W, Shi B (2018) Amphiphilic PA-induced three-dimensional graphene macrostructure with enhanced removal of heavy metal ions. J Colloid Interface Sci 512:853–861

Tang M, Yang TS, Zhang Y (2016) A brief review on α-zirconium phosphate intercalation compounds and nano-composites. Sci China Techn Sci 59:436–441

Theron J, Walker JA, Cloete TE (2008) Nanotechnology and water treatment: applications and emerging opportunities. Crit Rev Microbiol 34(1):43–69

Wiśniewska M, Wawrzkiewicz M, Polska-Adach E, Fijałkowska G, Goncharuk O (2018) Nanosized silica–titanium oxide as a potential adsorbent for C.I. Acid Yellow 219 dye removal from textile baths and wastewaters. Appl Nanosci 8:867–876

Wood GC, Hodgkiess T (1972) The hardness of oxides at ambient temperatures. Mater Corros 23:766–773

Wu ChY, Tu KJ, Deng JP, Lo YS, Wu CH (2017) Markedly enhanced surface hydroxyl groups of TiO_2 nanoparticles with superior water-dispersibility for photocatalysis. Materials 10:566–579

Zakutevskyy OI, Sydorchuk VV, Khalameida SV, Kovtun MF (2020) Sorption properties of bulk and deposited ammonium molibdophosphate with respect to Cs^+, Sr^{2+}, and $UO_2{}^{2+}$ ions. Theor Exp Chem 56(3):205–211

Zhang C, Lin C, Li C, Quan Z, Liu X, Lin J (2008a) Enhanced Luminescence of BPO_4 by Mixing with SiO_2 and Al_2O_3. J Phys Chem C 112:2183–2219

Zhang QR, Du W, Pan BC, Pan BJ, Zhang WM, Zhang QJ, Xu ZW, Zhang QX (2008b) A comparative study on Pb^{2+}, Zn^{2+} and Cd^{2+} sorption onto zirconium phosphate supported by a cation exchanger. J Hazard Mater 152:469–475

Zhuravlev LT (1987) Concentration of hydroxyl groups on the surface of amorphous silicas. Langmuir 3:316–318